AAS 23-156

DESIGN, INSTRUMENTATION, AND DATA ANALYSIS FOR THE SLS CORE STAGE GREEN RUN TEST SERIES

John H. Wall*, Chris Russell†, Richard K. Moore‡, Jeb S. Orr§, Abran Alaniz¶, and Stephen G. Ryan‖

The Space Launch System (SLS) Core Stage (CS) Thrust Vector Control (TVC) system is comprised of eight mechanical feedback Shuttle heritage Type III TVC actuators and four RS-25 engines, each attached to a Shuttle heritage gimbal block/bearing. The actuators are powered by a Shuttle-derived hydraulic Core Auxiliary Power Unit (CAPU), and integrated with an all-new Core Stage thrust structure. The actuators are interfaced to the SLS Vehicle Management (VM) software via an all-new TVC Actuator Control (TAC) avionics subsystem. Despite the significant test and flight experience of the Shuttle hardware, the SLS Green Run ambient and hot fire test activities revealed a number of new findings associated with the dynamic response of the TVC integrated system. Test responses suggested that the TVC system did not meet its performance specifications and its step and frequency responses exhibited unexpected departures from prior lab tests and modeled behavior. This paper is the fifth installment in a seven-paper series surveying the design, engineering, test validation, and flight performance of the Core Stage Thrust Vector Control system. In this paper, the design of the TVC analyses conducted during the Core Stage Green Run test series are discussed in detail. Throughout the course of the test activities, the SLS flight control team worked diligently with the Core Stage contractor to revise test command profiles and ensure sufficient instrumentation was available to collect data. Post-test analysis combined the Green Run modal, ambient, and hot fire test data, MSFC 2-axis Core Stage TVC Inertial Load Simulator (ILS) data, Hardware-In-the-Loop (HWIL) Systems Integration Lab (SIL) results, and actuator Acceptance Testing Procedure (ATP) responses. These data were used to characterize the response, validate critical math models of the TVC subsystem, and isolate the probable cause of the unexpected responses. Through comprehensive analysis of the available test data sources, the integrated team identified the dominant contributors to the observed response and developed test-correlated rationale for vehicle flight control system performance, ultimately leading to a confident posture for the Artemis I mission.

1 INTRODUCTION

The Space Launch System (SLS) launch vehicle flight control system commands eight core stage actuators to gimbal four RS-25 engines' thrust from liftoff to the RS-25 main engine cutoff (MECO) event. Prior to booster separation, the core stage Thrust Vector Control (TVC) system shares control authority with booster TVC but is the sole means of achieving attitude control in exoatmospheric

*SLS Flight Controls Lead, Mclaurin Aerospace (Jacobs ESSCA), Huntsville, AL
†Core Stage TVC Engineer, The Boeing Company, Huntsville, AL
‡Flight Systems Technical Staff, Mclaurin Aerospace (Jacobs ESSCA), Seattle, WA
§SLS Flight Dynamics and Control Technical Specialist, Mclaurin Aerospace (Jacobs ESSCA), Knoxville, TN
¶Flight Systems Principal Staff, Mclaurin Aerospace (Jacobs ESSCA), Houston, TX
‖SLS Chief Engineer's Office (MTS CPSS), Huntsville, AL

flight after booster burnout. Leveraging the heritage Shuttle actuators but cognizant of the new application on an entirely new SLS thrust structure, the MSFC in-house flight control team levied a set of key TVC requirements imposed on the stage contractor to ensure robust and stable vehicle flight control throughout its ascent flight. The flight companion paper[5] shows the frequency and transient response spec boundaries within which the the engine angular position must remain when commanded at small amplitudes.

Another key verification criteria is the load resonance frequency, which ensures adequate performance and stability of the TVC position control loop. Given a known moment arm and inertia, the load resonance frequency is primarily driven by the effective structural stiffness as "seen" by the actuator, necessarily excluding any compliances inside the actuator loop, such as that resulting from the hydraulic oil or actuator compliance measured by the mechanical position feedback linkages. Equation (1) shows a suitable approximation for the undamped load resonance frequency as a function of the engine inertia J_n, linear load stiffness K_L, and moment arm R. The engine rotational stiffness K_n is included for completeness here but has generally been found to be negligible due to the small loads imposed by propellant feedlines and associated hardware.

$$\omega_L = \sqrt{\frac{K_L R^2 + K_n}{J_n}} \tag{1}$$

This load stiffness (K_L) is the combined result of the stuctural compliances in each actuator's load path including the engine section support/thrust structure, the engines themselves, and the gimbal and actuator attach interfaces thereof. The load stiffness is a key quantity utilized in the TVC and flight control models for pre-flight stability and performance predictions, but determining its value from analysis often proves difficult, and few opportunities exist to accurately determine its value from testing.

Figure 1 shows the minimum load resonance frequency requirement. Since the SLS core stage thrust structure was designed to interface requirements conistent with those used for the RS-25 engine on the Space Shuttle Orbiter, the load resonance frequency was expected to fall above a minimum frequency value.

While the frequency response, step response, and load resonance frequency requirements apply to the fully integrated flight system under hot fire thrusting conditions, the Green Run represented the only opportunity to verify the SLS core stage TVC system performance in flight-like boundary conditions. This is in contrast to the Shuttle Main Propulsion Test (MPT) program conducted with a Shuttle Main Propulsion Test Article (MPTA) built solely for a comprehensive ground testing campaign.[1] Shuttle MPTA included an extensive series of ambient and hot firing tests with TVC commands spanning a range of amplitudes and waveforms.

Throughout the course of the SLS program, the NASA flight control and TVC teams sought to ensure the necessary testing was conducted to demonstrate that the design was compliant with the requirements and the linear TVC models were accurate representations of the SLS actuation subsystem. Through persistent efforts early in the program, the NASA teams worked to baseline a set of frequency and step vectoring commands and string potentiometer (string pot) based nozzle position instrumentation as a critical part of the Green Run Hot Fire test campaign. Integrating components of the newly-designed core stage, engine section, and hydraulic power system, the overall TVC verification and validation approach and the Green Run test series was managed by the stage contractor. Up until several revealing findings during the Green Run campaign, the contractor's official

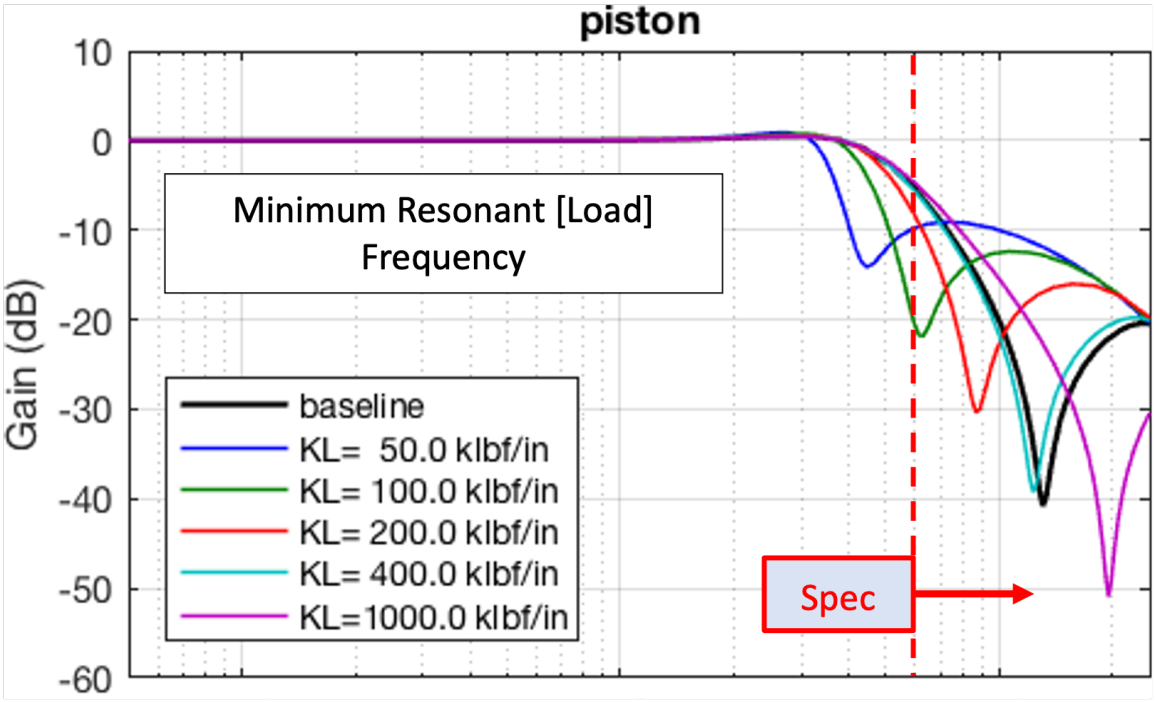

Figure 1. Minimum Load Resonance Specification

plan for closure of step, frequency, and load resonance requirements was solely via analysis. The analysis was largely based on traditional single-axis TVC models, with limited validation through laboratory testing. The NASA flight control and TVC engineers worked diligently over the course of the SLS program to maintain engagement with the contractor's modeling, test, and analysis activities, ultimately leading up to Green Run hot fire. In the end, the engineering collaboration and active communication between NASA and the contractor teams proved to be essential in ensuring that test coverage was adequate and post-test analysis was successful.

Prior to the Green Run test activity, and based on extensive NASA MSFC experience, the flight control and TVC teams relied primarily on a planar, linear, small-signal approximation of the TVC dynamics known as the Simplex model (A "Simpler" version derived from the multi-servo-channel "Complex" model). The Simplex model, represented equivalently in block diagram form, linear state space, and compiled language simulation environments, is largely based on first principles with some linear approximations. Since Shuttle flight data and Saturn experience did not suggest any significant friction-induced Limit Cycle Oscillations (LCOs), and the same Shuttle gimbal bearings and engine technologies were re-used on SLS, the MSFC flight controls community was confident through the design process that the in-flight vibration environment would render friction effects negligible. As such, friction effects were generally excluded from TVC and flight control analysis during the SLS program. Lacking flight-like thrust loading, laboratory testing with single-axis test stands and vendor acceptance test procedures (ATP) did not exhibit friction effects. The vendor and lab data routinely demonstrated excellent agreement with the linear simplex representations accross the range of frequencies relevant for flight control analysis, in part due to the precision engineering and design-for-linearity inherent in the Orbiter heritage actuator hardware (exclusive of gimbal bearing friction).

As will be discussed in the sections that follow, the extended testing accomplished by the MSFC 2-axis inertial load simulator laboratory and the ambient and hot fire vectoring tests conducted at Green Run challenged the long-standing assumptions present in the Simplex model, particularly with respect to structural stiffness and gimbal bearing friction. The effects of gimbal friction were pronounced during hot fire. The load resonance frequency, while falling above the 6 Hz requirement in all conditions tested, was significantly different in the thrusting and non-thrusting conditions. In addition to the unexpected results, data from both tests showed violations of the step and frequency response requirements. Following the test series, a comprehensive analysis revealed that several model refinements were required to represent the observed behaviors.[3,4] The team recommended acceptance of the requirement violations (specific to Artemis I) by showing that test-anchored bounding model predictions of a Limit Cycle Oscillation (LCO) would not present a risk flight. The pre-flight analysis and the results of the highly successful first flight of Artemis I are discussed further in a companion paper.[5]

2 MSFC 2-AXIS INTERIAL LOAD SIMULATOR LABORATORY TESTING

The stage contractor and the MSFC NASA TVC team shared the responsibility of contructing a test fixture to evaluate the integrated Core Stage TVC system, with as much flight hardware as practical, prior to Green Run testing. At the MSFC 4205 TVC test lab, the NASA engineering team built a fully functional 2-axis Inertial Load simulator (shown in Figure 2) whereby two RS-25 actuators gimbal a simulated engine about a flight-like Orbiter heritage gimbal bearing. The backup/thrust structure stiffness is simulated with a cantilevered plate to which the tailstock of the actuator is attached and torsional rods are installed between the test stand and the engine simulator to approximate the engine proplleant feedline loads. The flight-like or flight-equivalent hydraulic actuators were powered by either a facility hydaulic system or a flight hydrogen-driven Core Axilliuary Power Unit (CAPU), the evaluation of which was a major subsystem qualification objective of the laboratory test campaign. Commands were sent to the actuators using either the Shuttle heritage analog Portable Command Signal Controller (PCSC) or flight-like TVC Actuator Controllers (TACs). In the case of the TACs, a flight software emulator or the actual flight software running next door in the Systems Integration Lab, the SLS HWIL facility,[6] issued pitch/yaw angle commands. Flight-like telemetry and lab-specific instrumentation data was collected in the lab environment, including linear encoder measurement of the actuator stroke, string pot-based inertial load position, tailstock-mounted load cells, as well as the available on-board piston position (actuator stroke) measurements, command currents, and angle commands to be used in Green Run and post-flight analysis. The lab instrumentation was collected at 1.0 kHz, time-synchronized to the flight-like telemetry at 50 Hz, and provided to the flight control team in a form ready for analysis.

2.1 Early Development Testing

The 4205 2-axis test stand provided the SLS engineering team high confidence in the efficacy of the Green Run test approach both in commands and instrumentation. Early testing enabled the engineering team to confirm the behavior and suitability of the modeled TVC system response in the relevant environment as well as demonstrate the process of uniquely identifying model parameters from test data. Figure 3 shows the frequency responses using the Green Run Hot Fire command sequence when the lab was configured in 2017 with Shuttle MPTA heritage Type III actuators. A sequence of sinusoidal and step commands identical to the planned Green Run vectoring profile, were sent using the analog PSCS controller. The linear encoder (actuator stroke), on-board piston

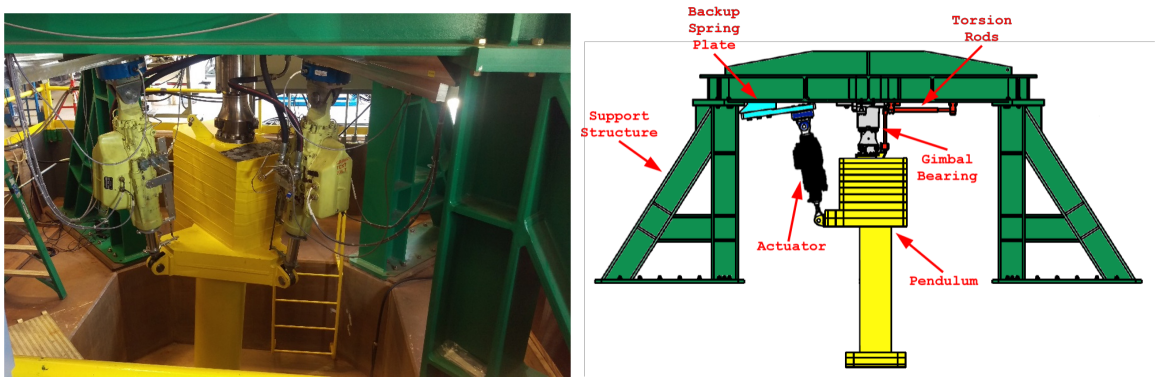

Figure 2. NASA MSFC 4205 2-Axis Inertial Load Simulator Test Stand

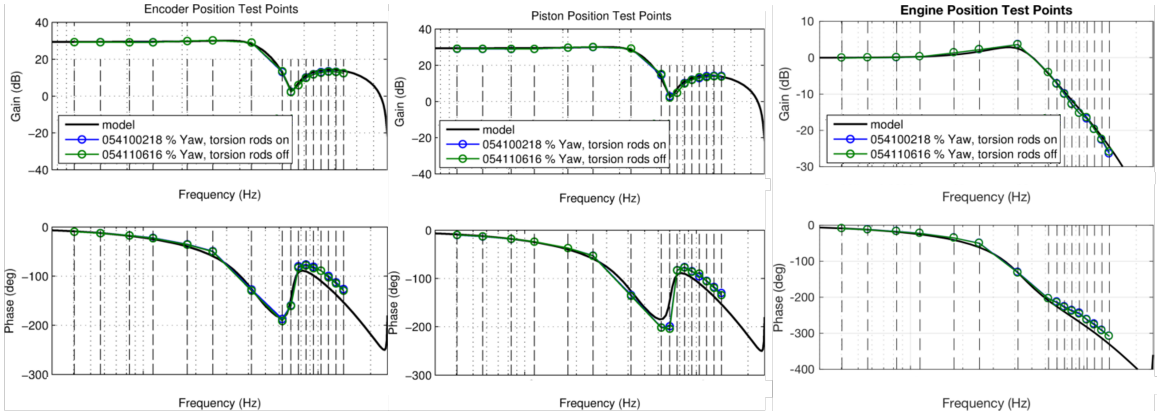

Figure 3. 4205 Lab Early 2017 Frequency Response Using Green Run Style commands

position (strain gauge based, telemetered), and nozzle results (string potetiometer derived) is shown. Using this test data and the linear model representations, the engineering team was able to determine the load parameters from frequency response, adjust the linear model accordingly and achieve agreement between modeled and lab-measured response. Since the moment arm and load inertia are very accurately known, the load stiffness can be determined from the load resonance frequency using Equation (1).

While the actual value of the load stiffness was found to be softer in the lab than calculated for the cantilevered beams prior to the build, the lab demonstrated the efficacy of the Green Run test approach to determine the critical system parameters, and confirmed the ability of the planar, linear TVC models to predict the system responses.

Even though the linear models fit the frequency response extremely well, further testing with a series of triangle wave ramp testing and load cell-based analysis were conducted to identify possible sources of friction in the gimbal joint, and confirm negligible friction in the ambient (free-hanging) configuration. As expected, the data suggested that other small-amplitude phenomena (such as small-signal nonlinearities in the actuator and roll coupling with the inertial load simulator, whose roll inertia was significantly less than the flight nozzles) far exceeded any measurable effects of friction. Step testing was also conducted at a range of amplitudes including the ranges considered for Green Run hot fire testing (0.6, 0.4 and 0.2 degrees), demonstrating a match with linear

models as shown in Figure 4. At higher amplitudes, the responses appeared to match better than the lower amplitudes. This was especially true for the nozzle position, which consistently showed increased overshoot compared to the model as well as some variable steady-state offset behavior. This amplitude-dependent effect, seen in the lab step responses, was later observed during ambient testing at Green Run and remains the subject of investigation. It is thought to be the result of gimbal bearing mechanical clearances and power spool overlap in the actuator.

2.2 Subsystem Qualification Testing

The core stage contractor's use of the test lab was primarily for providing a suitable environment for integration testing of the hydrogen-driven CAPU, which provides hydraulic power to the actuators. This test, known as Subsystem Qualification Testing or Subsystem Test Article (SSTA) testing, was largely conducted prior to Green Run ambient testing, but the lab configuration remained until after Green Run for further testing based on its outcomes. The lab setup for SSTA utilized flight-like TACs which were commanded by a flight software emulator also used during assembly at the Michoud Assembly Facility (MAF). Apart from the command avionics update, the lab was largely unchanged from the 2017 testing with the exception that the actuators used where Shuttle surplus Type II actuators, which have different actuator feedback and command gain parameters than the Type IIIs previously tested (and installed on SLS). Due to multiple configuration changes and a transition in test management from NASA to the stage contractor, the first indications of a TAC electronics amplitude-dependent gain offset (nonlinear scale factor) went unnoticed until the first tests at Green Run. Figure 5 shows the linear encoder (actuator position) and string pot-based engine position response from the SSTA lab environment against the model with the Type II actuator parameters updated. While the piston notch frequency and peak response are consistent with prior lab responses as expected, both quantities show a noticeable reduction in gain, later found to be the result of a crossover distortion in the TAC's analog servo amplifier.[5]

3 GREEN RUN AMBIENT TESTING

3.1 TC-5: Engine Modal Testing

During the preparations to install the SLS Core Stage into the B-2 test stand, structural dynamics instrumentation was installed to facilitate modal testing with the empty core stage hanging from its handling interfaces, suspended on a support crane. During this test, the flight actuators were installed but inoperative, and "locked" using a Shuttle Orbiter heritage mid-stroke lock device, a steel collar that precludes motion of the rod with respect to the actuator body by coupling the rod to the body at the end of the hydraulic cylinder. Modal identification attempted to determine the *locked* pendulum modes, i.e., the load resonance of the uncommanded, empty engine with a "rigid" actuator in an effort to provide supporting evidence to verify the flight control load resonance frequency requirement. However, this test suggested that the engine pendulum modes were lower than expected.

Due to inconclusive identification of the pendulum modes, an engine section modal test, conducted by NASA, was implemented along with additional MSFC instrumentation after the core stage was installed into the B-2 test stand (Figure 6). The resulting responses confirmed the lower than predicted first pendulum mode frequency observations during crane testing, although results were still inconclusive, because no analysis or testing had been performed to determine the compliance of the mid-stroke lock hardware. After the mid-stroke locks were removed, the accelerometers

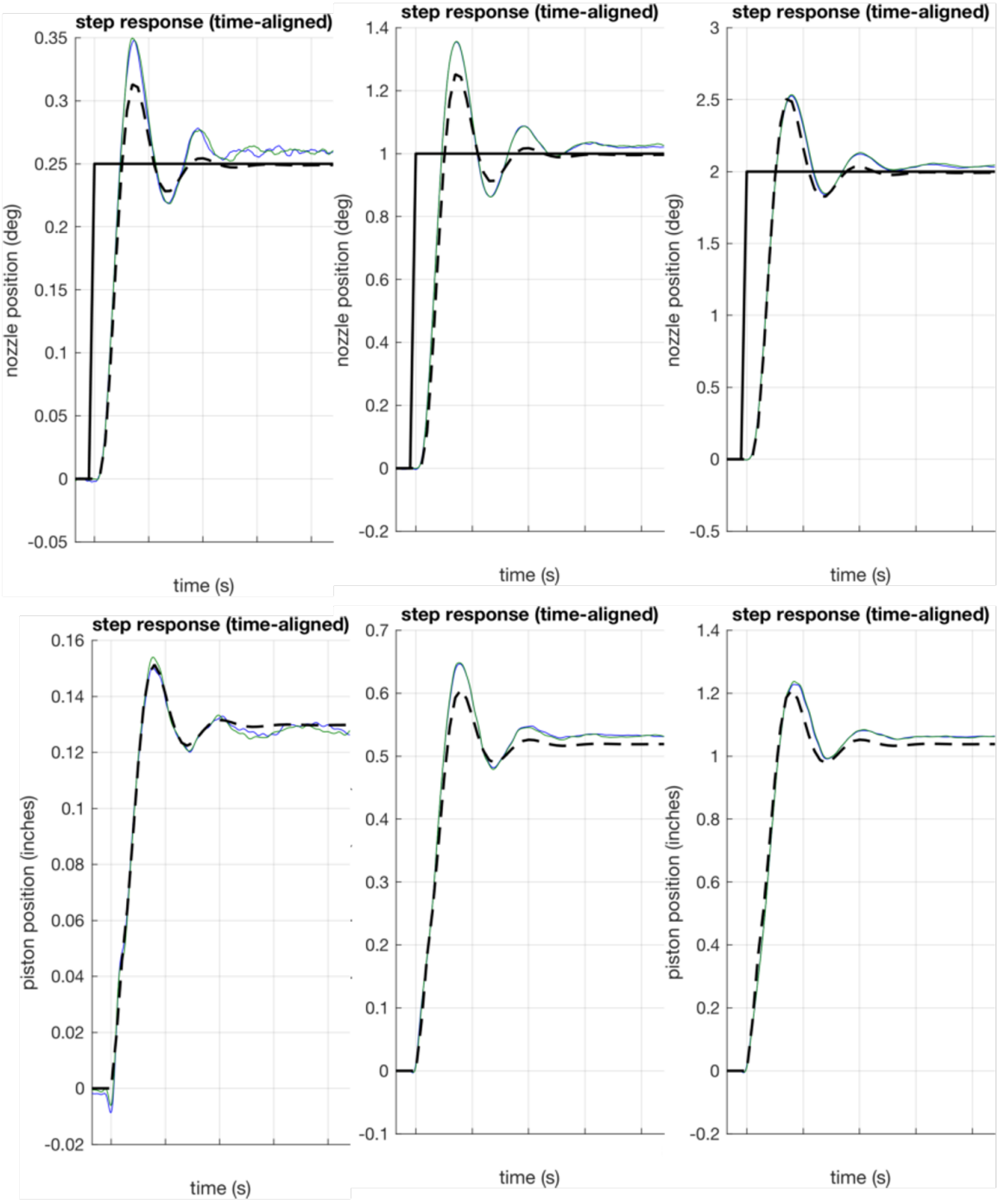

Figure 4. MSFC 4205 2-axis ILS Test Lab, 2017 Step Responses

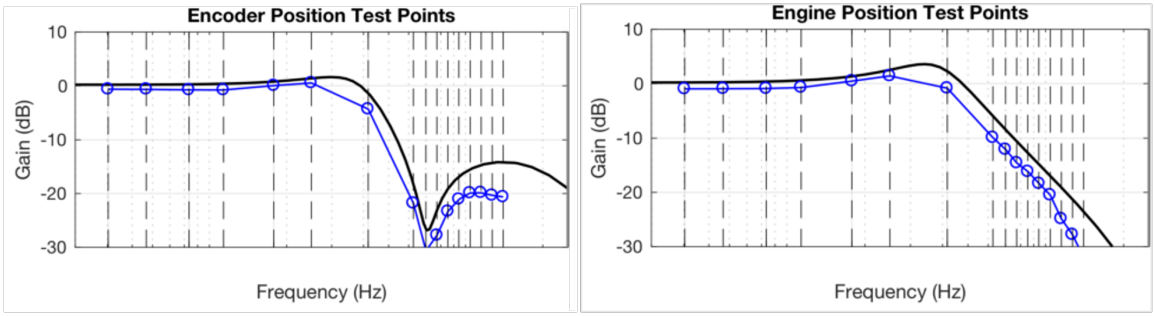

Figure 5. MSFC 4205 2-axis ILS Test Lab, 2020 SSTA Frequency Responses

used for modal ID (including several on the engines) remained installed during the TC-5 initial vectoring test.

The TC-5 vectoring test's primary objective was verification of the the minimum load resonance requirement. However, this test approach was complicated by the fact that the active damping of the actuator makes the pendulum mode nearly unobservable, and that the pendulum mode (which depends on the total compliance) and the load resonance (which excludes the oil) are not at the same frequency. The NASA TVC team initially expected that the closed-loop position feedback would damp the pendulum mode, but the instrumentation and Operational Modal Asssesment (OMA) detected a clear pendulum mode just above the spec minimum load frequencyduring the 20 minute quiescent period prior to vectoring.[7] After revisiting static loading data from the actuator vendor and determining that the piston displacements were below the telemetry quantization thresholds during this 20 minute period, the NASA TVC team concluded that the subject modes were due to engine motion within the actuator's servo or power spool deadbands (estimated to be larger than the piston quantization limit). This implied that the observed mode involved the actuator oil column in series with the rest of the engine, gimbal, and stage structure, *viz.*, the pendulum mode. With a recommendation from NASA TVC based on the known feedback characteristics of the actuator (i.e., nulling of the oil column compliance when servo is out of deadband), the core stage contractor closed the load resonance verification under the assumption that the load resonance must be strictly greater than the observed pendulum mode; that is,

$$\omega_L > \omega_T = \sqrt{\frac{K_T R^2 + K_n}{J_n}} \tag{2}$$

where

$$\frac{1}{K_T} = \frac{1}{K_L} + \frac{1}{K_{\text{oil}}}. \tag{3}$$

This expression is similar to the load stiffness Equation (1), except that the relationship describes the total resonance frequency (engine pendulum mode frequency) ω_T, as a function of the combined total stiffness, K_T, where the total stiffness results from the oil stiffness, K_{oil} in series with the load stiffness K_L .This approximation assumes that the load stiffness is suitably represented by a single spring, K_L, and that the inertia and moment arm are precisely known. However, further analysis suggested that a single-spring approximation in any test configuration (mid-stroke locked, within deadband) could not be conclusive evidence of the load resonance. This is because load resonance is influenced by a dense spectrum of engine pendulum-type modes that involve

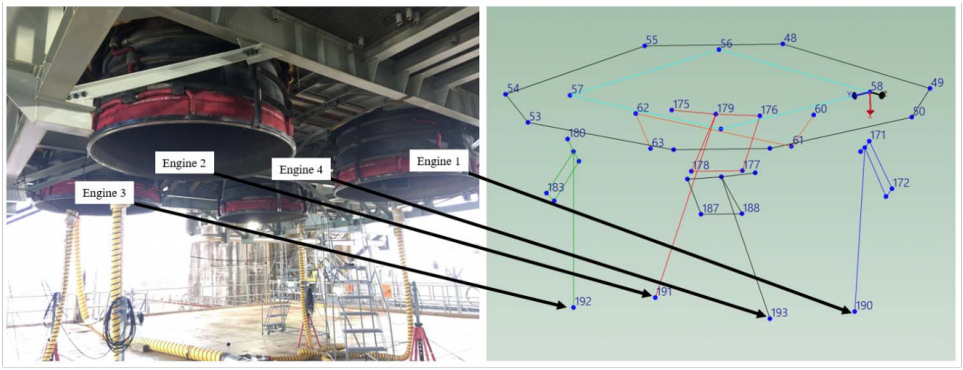

Figure 6. TC-5 Accelerometer Locations

heavy thrust structure participation and their integrated effect provides an equivalent single-valued observed load stiffness.[4] In other words, the total resonance frequency does not necessarily correspond to any given frequency peak in a modal test. A final note regarding the TC-5 model test was that the mid-stroke locked actuator first engine pendulum modes appeared to fall close in frequency to those detected during the quiescent period where actuator acted like a column of oil. While an independent measure of neither the oil nor locked stiffness was available, the frequency match provided some corroborating evidence that the oil column stiffness was similar to the locked actuator stiffness. This provided supplementary verification that the hydraulic fluid's air entrainment was sufficiently low to ensure that the oil column stiffness was in the predicted range .

3.2 TC-5: First Gimbaling of Integrated Core Stage

Vectoring tests of the TVC system on the integrated stage were initially to be performed following assembly of the core stage at Michoud Assembly Facility (MAF). However, due to limitations associated with the transition from vertical to horizontal assembly, the first commanded motions of the engine nozzles on the integrated vehicle were performed after the stage was installed vertically in the Stennis Space Center (SSC) B-2 test stand. The vectoring test at B-2 provided was advantageous because the string pot instrumentation used to determine engine angular position was connected to the SSC data acquisition system. This string pot data provided early indications that additional ambient testing prior to the hot fire vectoring test was needed.

The series of TVC vectoring commands issued during this test were similar to the basic frequency and step response commands as executed during the Shuttle Program in the Orbiter Processing Facility prior to each Shuttle flight.[1] Step and frequency commands were individually issued to each actuator with an amplitude of 0.25 deg at the flight control command rate of 50 Hz (every 20 ms). The frequencies were a set of four discrete sines as follows. These commands were executed one engine at a time on September 9, 2020, as shown in Figure 7.

- 0.25 deg, 0.1 Hz, 25 cycles (250 seconds)
- 0.25 deg, 0.2 Hz, 25 cycles (125 seconds)
- 0.25 deg, 1.0 Hz, 25 cycles (25 seconds)

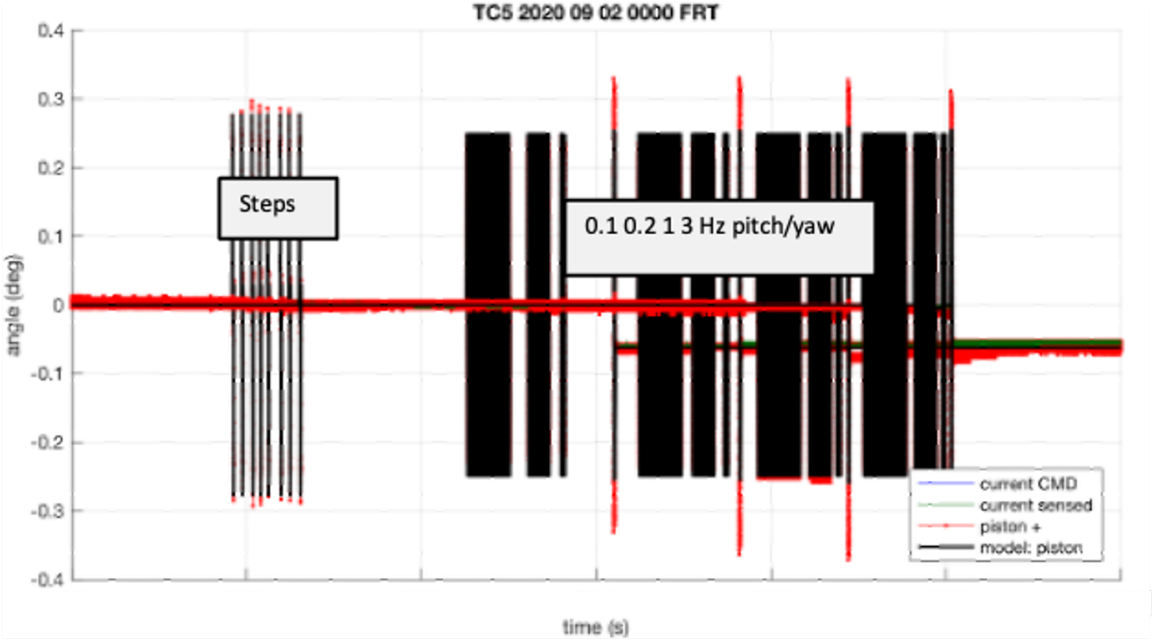

Figure 7. TC-5 Commands

- 0.25 deg, 3.0 Hz, 25 cycles (8.333 seconds rounded to 8.32 seconds)

The key TVC response measurements available during the test included the commanded current (Amps), sensed current on the actuator servo-valves (Amps), piston position (inches), and string pot lengths (inches). For convenience in comparison, the currents and piston positions were converted to degrees using simple scalings. Additionally, the string pot lengths were transformed into engine angles in degrees, although required more involved transformations due to the geometric placement of sensor end points. Comparing the commanded current, piston, and string pot-derived engine responses to the pre-test models immediately revealed a number of findings. Note that the last commanded value is nonzero due to the final 3.0 Hz cycle not falling on an integer sample boundary.

The string pot data was inadvertently recorded at 1 Hz instead of the target 250 Hz data rate during the steps. This meant that transient response characteristics of the nozzle could not be observed. During the slower full sweep commanding, and during the steady-state step response portion where 250 Hz string pot data was recorded, the string pot end point location data (according to the attach point drawings) did not provide a suitable length-to-angle solution that sufficiently corroborated the piston response. As is discussed further in Section 5.1, the available attach locations for string pots led to a solution space highly sensitive to knowledge of end point locations.

Figure 8 shows the positive (extend) and negative (retract) step response for the current commands, current sensed, and piston response along with the pre-test models that assumes a load stiffness of around 450 klbf/in. The response reveals two major characteristics that did not match the pre-test expectations. One is that the current sense telemetry, representing the actual servo-valve current to the actuator torque motor, does not follow the command received by the TAC and shows an offset. The other is that the piston response shows a consistently larger overshoot than predicted by the model driven by the sensed current. The steady-state piston position follows the sensed current offset, indicating that the sensed current is representative of the current going to the

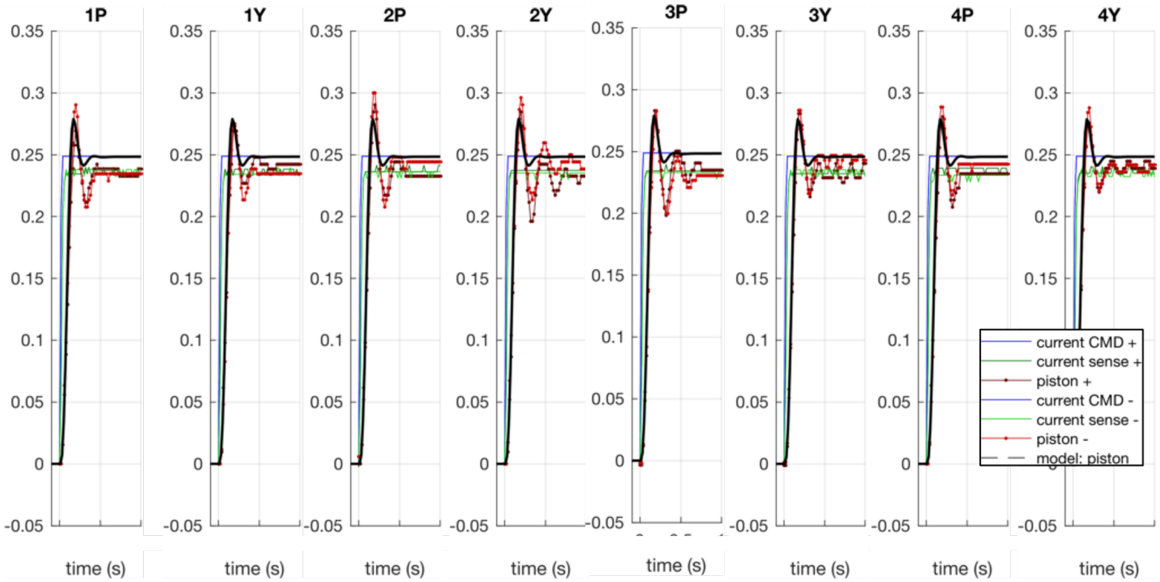

Figure 8. TC-5 Step ResponseTC-5 Commands, Degrees

servovalves.

Figure 9 shows an overlay of the negative and positive current and piston responses for each step doublet against the TVC nozzle step response specification. While a piston boundary is not defined, the nozzle dynamic response is always larger. Thus the clear violation of the nozzle envelope by the piston response provided an early indication that the nozzle step response requirements would not be met. The overlay plots indicated a fairly consistent response between the positive and negative steps and confirmed that all the engines behaved similarly.

Figure 10 shows the results from the discrete sine frequency response reconstruction technique (described in Section 5.2). The piston data shows peaking consistent with the step overshoot and both responses demonstrate the -0.5 dB of gain reduction consistent with the steady-state offset observed in the step responses. While string pot data was recorded at the full target rate during the frequency responses, the angle solutions were not reliable due to the uncertainty in the end point locations, which produced a large amount of variation in the results.

In addition to the piston and current data, engine accelerometer data (recorded at 512 Hz), as well as video data, was used to confirm that the nozzle motion during steps was indeed exhibiting an underdamped response. Figure 11 shows accelerometer responses from each of the steps along with the Simplex TVC response model of the near-exit plane aft accelerometer locations. The increased overshoot seen between the model and the accelerometer data confirmed the responses observed in the piston data.

Parametric sensitivity studies were performed using the Simplex model in an effort to determine possible explanations for the underdamped response. Hand tuning of model parameters to fit the observed responses and iterative optimization methods led to a number of possible mechanisms, including different than expected mechanical component parameters, a slightly different moment, abnormally high oil compliance, or a lower-than-expected backup structure stiffness.

Based on the lack of engine position response data during the TC-5 test, and inconclusive nature

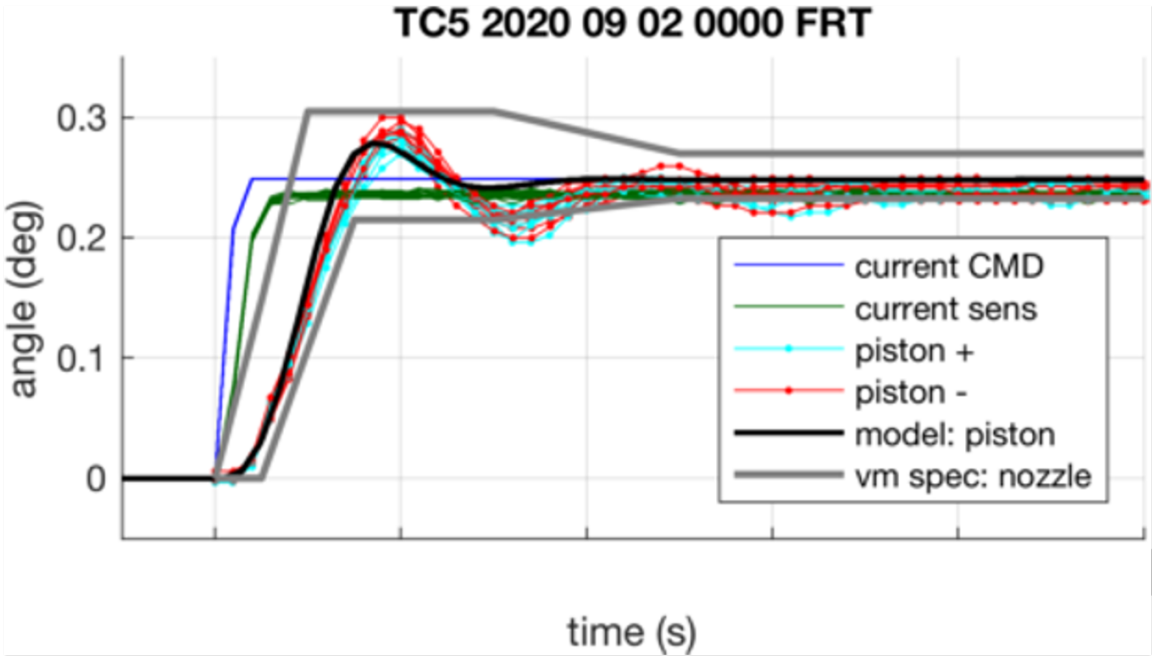

Figure 9. TC-5 Step ResponseTC-5 Commands

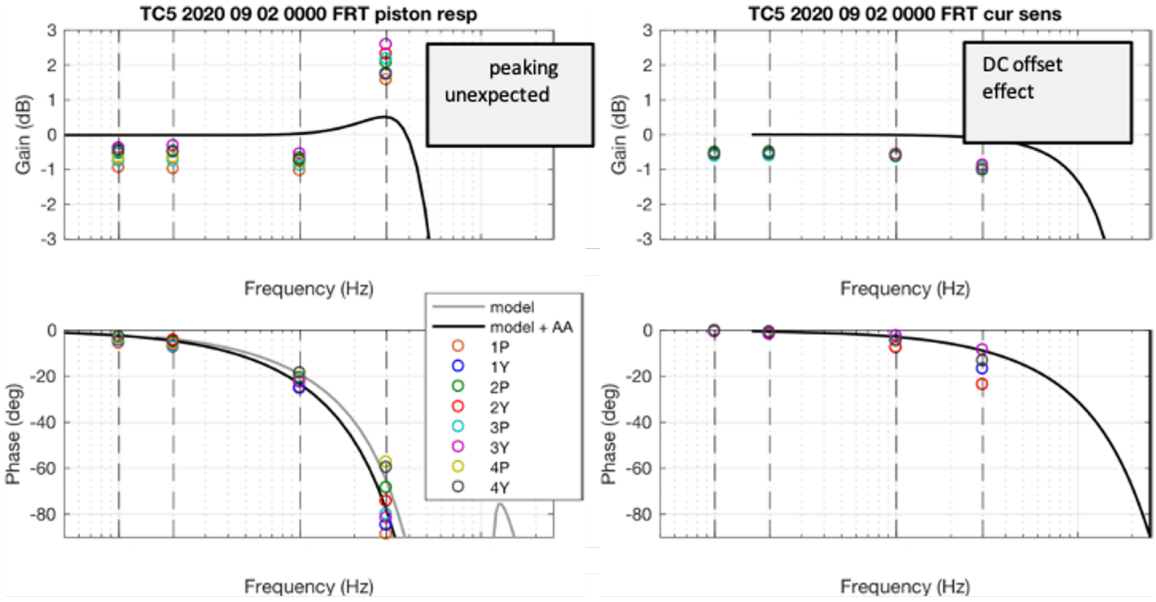

Figure 10. TC-5 Frequency Response Piston (Left), Current Sense (Right)

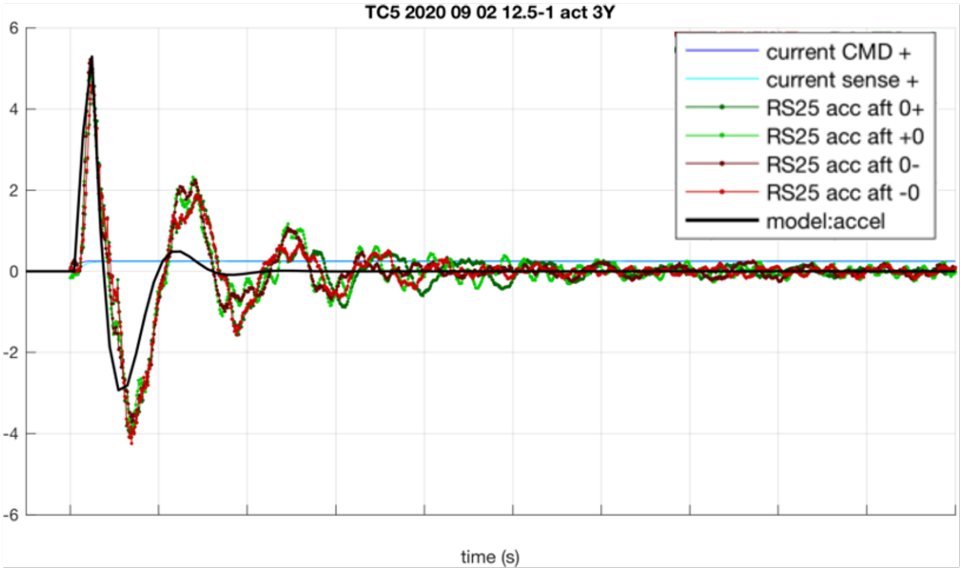

Figure 11. TC-5 Accelerometer responses during steps

of the limited test points, the NASA TVC team campaigned to add testing that would determine the cause of the observed behaviors and ensure that the string pot-based measurements were properly anchored prior to hot fire testing.

3.3 TC-7: Ambient Re-Test

The additional test activities described in this section, known as TC-7 conducted on 2020 Nov 30th, were not part of the original Green Run test plan. This was the only test, however, that isolated the value of the ambient condition load resonance. Based on piston measurement responses, this load resonance frequency (and corresponding load stiffness) was found to be much lower than in the pre-test model, which provided an explanation for the overshoot in the step response. The additional visual and string pot instrumentation provided a conclusive measure of engine motion, and altogether the discrepancies with respect to the expected TC-7 ambient response could be primarily isolated to the change in load stiffness from pre-test expectations. From this point, the team confidently proceeded to hot fire testing while performing impact assessments for flight with the lower load stiffness parameter.

3.3.1 Additional instrumentation Due to the geometric arrangement of the string pots, resulting from the available mounting points in the engine section, the ability to convert from sensed lengths to engine angles was very sensitive to string pot sensor end point knowledge. After requested by the flight control team, an instrumentation contractor utilized structured light photogrammetry to measure the precise location of each string pot sensor end points as well as the gimbal and actuator attach locations. Additionally, the contractor installed a 12 camera optical motion capture system and fiducial markers on the engine and engine section during testing, which provided a photogrammetric estimate of the engine angle. Finally, the test procedure was revised to ensure high speed recording throughout the duration of vectoring. While the visual system performed extremely well to confidently determine the engine angular position, the string pot data still showed significant scatter in the data despite incorporating measurements of the end points. The team explored a number of solutions to determine the best fit of the TC-7 string pot data and those solutions at the time are

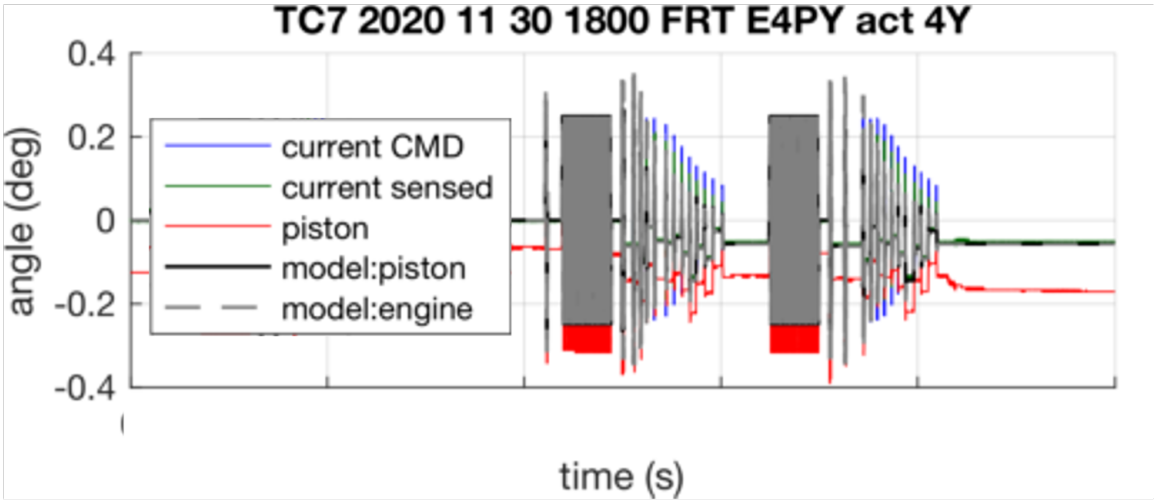

Figure 12. TC-7 Commands

represented in the ambient test results shown herein.

3.3.2 Additional Commands In an effort to minimize test time while also acquiring the essential data, the team coordinated with the stage contractor test leads to determine an additional set of vectoring commands. Unlike the pre-defined hot fire vectoring commands which allowed for commanded angular rate to exceed the normal flight rate limits, the commands during this test were software rate limited and issued individually by the stage controller. Engines 1 and 4 were chosen for testing as those engines contained the two types of actuator attachment configurations (inboard and outboard actuator tailstock mountings). Frequency responses were conducted both for indivudal pitch, yaw, and simultaneously commanded axes for combined axis engine motion to isolate any coupling behaviors. Steps of 0.25 degree were performed again, as in TC-5, but with an additional command amplitude of 1 degree (albeit rate limited by the commanding software). The commanded frequencies (up to about 15Hz), amplitudes (less than 0.25 seconds) , and durations (25 or greater cycles per command) were manually sent to the actuators one by one.

3.3.3 Processing A representative test response is shown in Figure 12. Post processing of this data required determining the start time of all the various sinusoids issued on the timeline, which was made possible by the availability of the telemetered commanded input data. The piston data shows an offset, whose slowly varying component results from thermal drift of the actuator as well as measurement error bias.

3.3.4 Response The 0.25 deg piston position responses compared well to the TC-5 responses, which demonstrated consistency between the test configurations. Figure 13 shows the frequency response from the pitch actuator command to the piston measurement in comparison to the pre-flight TVC model. The expanded range of frequency commands revealed the lower than predicted characteristic load resonance notch frequency, which had not been fully observable during TC-5.

The left plot in Figure 14 shows the measured piston frequency responses compared to the model with an adjusted load stiffness parameter. The right plot in Figure 14 shows the engine frequency

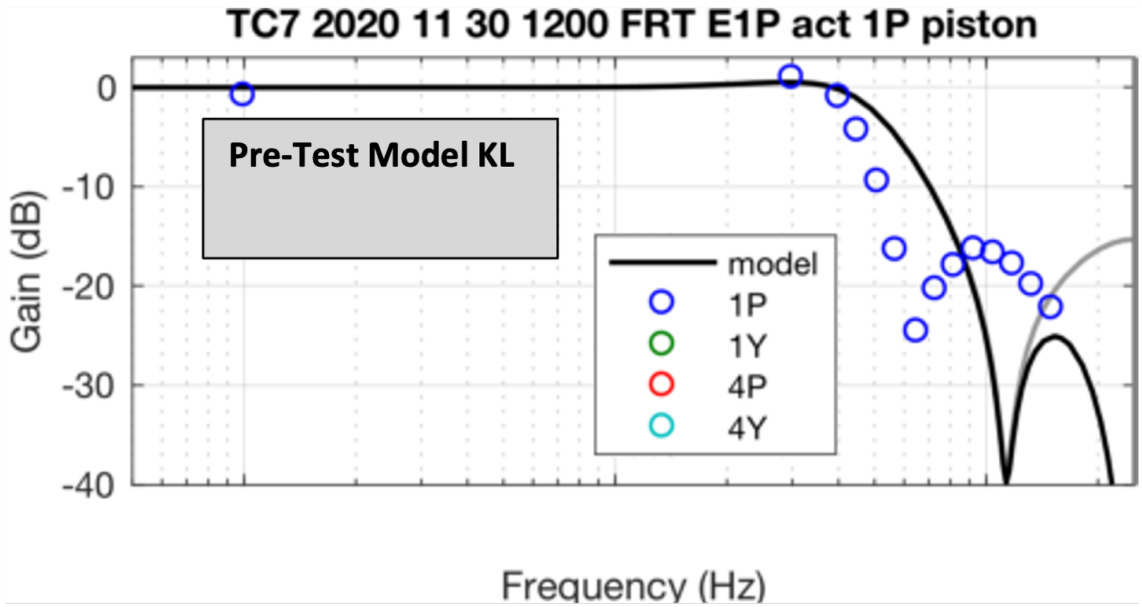

Figure 13. TC-7 Piston Frequency Response vs Pre-Test Model

response processed from the visual system data, showing a fair match to the response in peaking and corner frequency. As can be seen, the overshoot region of the response is clipping the upper boundary of the specification. Both responses show a deviation from the model in the higher frequency region, which was later attributed to the aforementioned scale factor error in the TAC command electronics.[5] While not shown in this paper, the combined axis frequency responses are similar to those for the individually commanded axes.

Figure 15 shows the step responses for the 0.25 deg commanded piston (left) and engine angle data (right). The piston data closely matches the adjusted model with the exception that it appears to track the steady state response of the current sensed value. The engine angle data shown on the right figure is derived from both the best-estimate of the angles from the string pot solution (gray) and the visual data (green colors). The visual data shows a similar trend to the piston steady state response in that the mean of the responses fall below the 0.25 deg commanded value. The string pot data is much more scattered than the visual data owing to the difficulty in determining absolute value from the geometry sensitivity of the string pot end points, even after the as-installed end point measurements were incorporated.

In an effort to eliminate the offsets due to the command avionics as well as reduce the scatter in the engine angle data, Figure 16 shows the same result but with the responses normalized to their individually achieved steady state values. While the piston data shows a fair match between the test and model responses, the engine responses according to the string pots and the visual data fall significantly out of bounds and do not agree with the model. Despite the mismatch between the test and model engine responses, the normalized step shows that the string pot reconstructed angle and the visual systems were in sufficient agreement to allow for useful transient data to be collected from the string pots during the hot fire test.

Figure 17 shows the responses from the one degree steps. While the one degree step responses were software rate-limited, the response comparison to the purely linear model and normalized

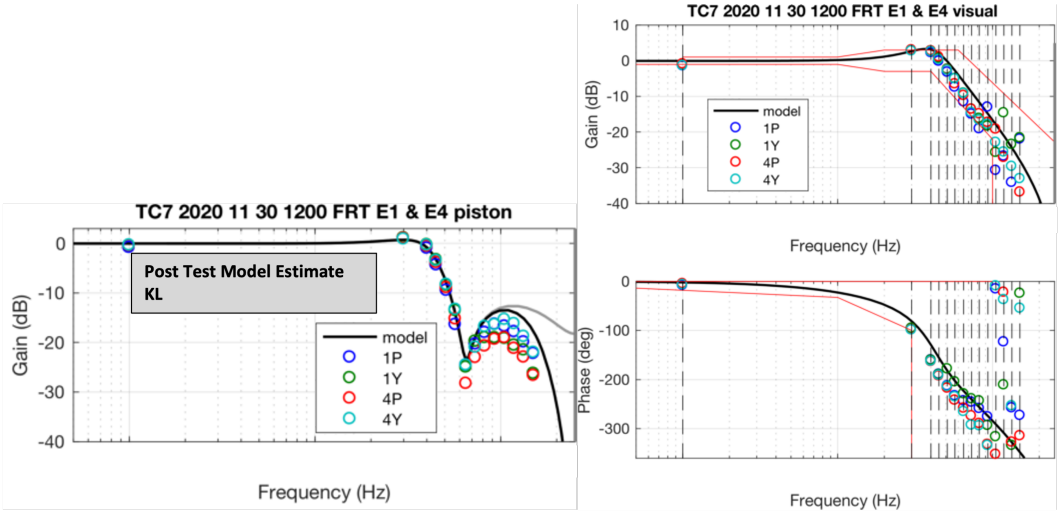

Figure 14. TC-7 Piston (left) and engine (right) Frequency Response vs Post-Test Model

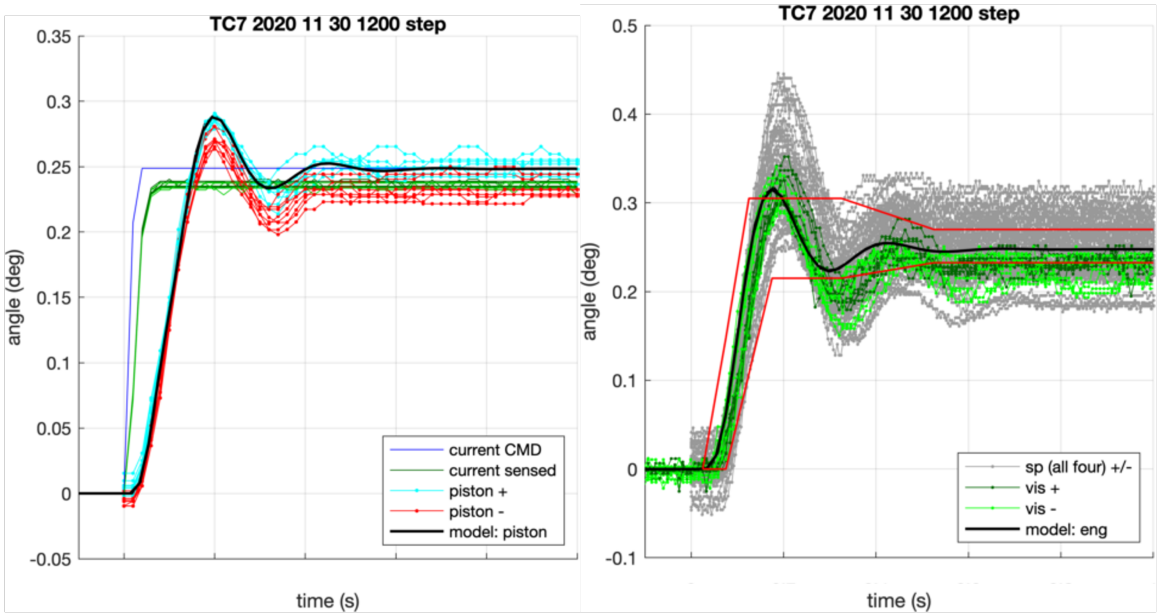

Figure 15. TC-7 Piston (left) and string pot (sp) and visual (vis) based engine (right) 0.25 deg response vs Post-Test Model

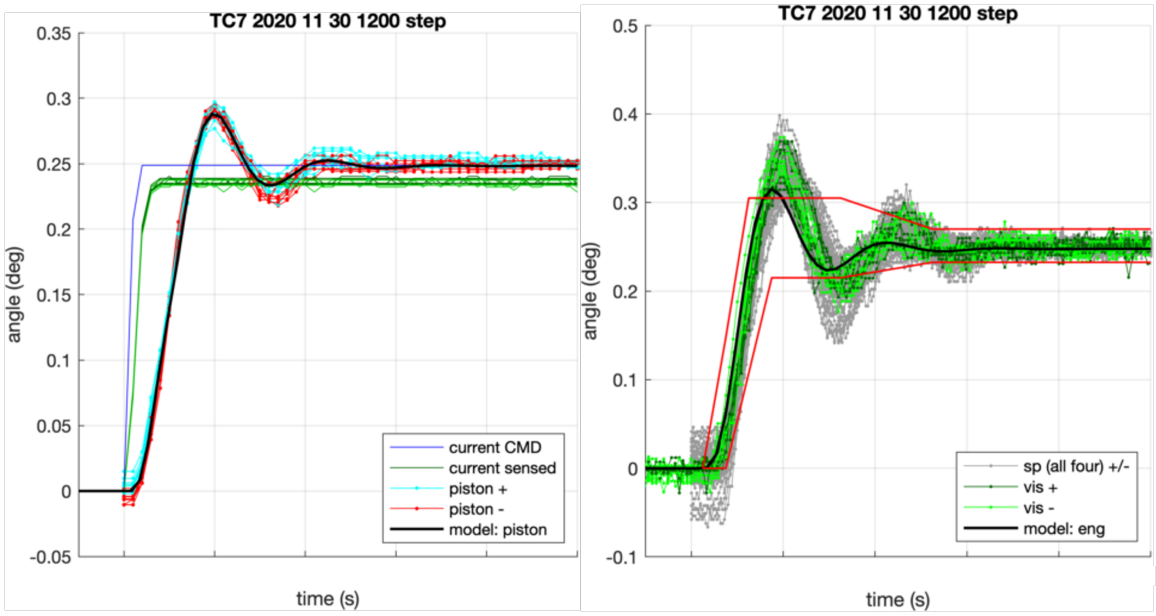

Figure 16. Normalized TC-7 Piston (left) and engine (right) Frequency Response vs Post-Test Model

spec bounds gives an indication of amplitude dependence outside of the rate-limiting regime. The piston and engine responses show less steady state error than seen in the 0.25 degree steps. This can be at least partially attributed to the nonlinearity asssociated with the command avionics but is also consistent with prior lab response trends, pointing to small-amplitude nonlinearities in the gimbal and actuator itself. The engine responses obtained from the camera system ("vis" labeled) indicate a tighter band of traces and a closer match to the model. While the scatter in the string pot measurement is a smaller percentage than for the 0.25 degree commands, there are some outliers not fully represented by the visual system results. During the processing of the hot fire string pot responses (Section 4), additional techniques were applied to the string pots that improved the angle solution (see Section 5.1) yet they relied on the same fundamental assumption made during TC-7 process: that the engine angle moved fully to its final commanded position. While the hot fire string pot to angle method still could not determine absolute engine position from the measurements, those methods would likely improve the scatter in the string-pot derived results shown here.

4 GREEN RUN HOT FIRE TESTING

The first Green Run Hot Fire (GRHF) was conducted on Janurary 16, 2021 but due to a test-specific monitored condition threshold violation, the engines were advanced to shutdown prior to reaching the period in which the engines were gimbaled.

The second and final SLS Green Run Hot Fire test was conducted on March 18, 2021, completing its full duration and providing valuable data and ultimately confidence for flight. The results of the Green Run hot fire test provided TVC response data that was significantly different than the ambient results: exhibiting much more damped response without any step overshoot and a piston response showing a higher apparent load resonance. The results gathered from hot fire testing challenged long-standing assumptions about the RS-25 gimbal friction and structural characteristics of the gimbal.[3–5]

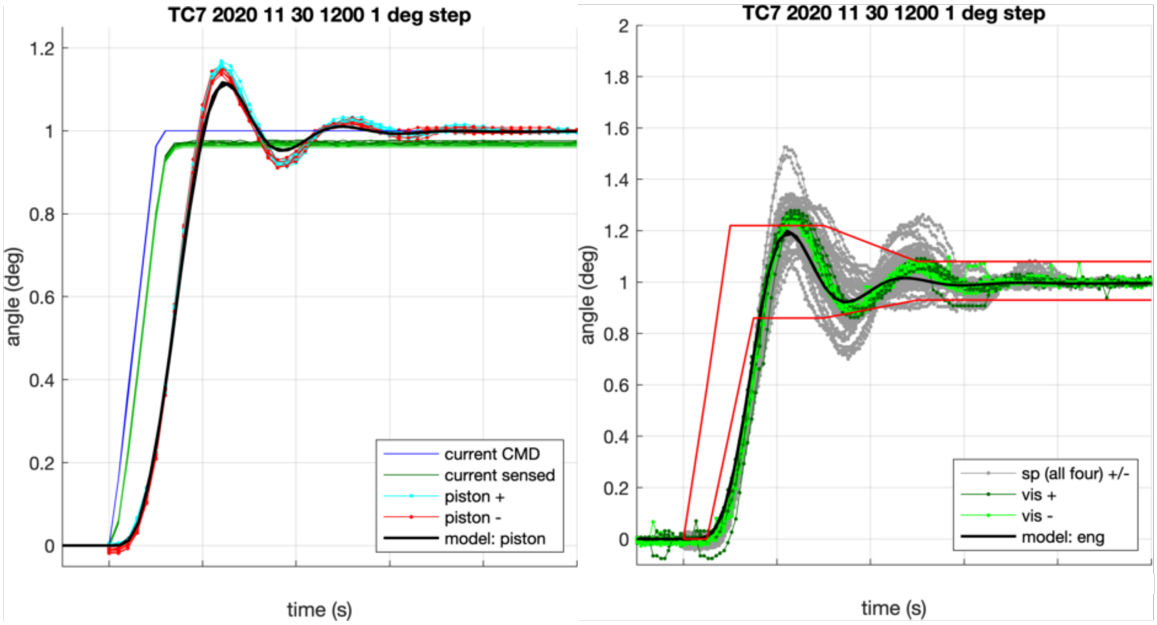

Figure 17. TC-7 Piston (left) and engine (right) Steps vs Post-Test Model

4.1 Commands and Instrumentation

The Green Run hot fire commands were executed by the Green Run vehicle flight software, which read a pre-loaded actuator command table and issued them at 50 Hz through the normal flight software interface to the TVC actuators. For the Green Run hot fire test specifically, the command amplitude and software rate limits were increased to allow the high-frequency test points to achieve sufficient amplitude for an adequate signal-to-noise ratio after attenuation by the acutator dynamics. Since only 120 seconds of test time was available for vectoring, the discrete pitch and yaw frequency response commands were sent simultaneously to all eight actuators but with high and low frequencies scheduled to minimize pitch/yaw cross talk. The steps were comprised of three amplitudes: 0.6, 0.4, and 0.2 degrees, and were issued to all yaw actuators, followed by all the pitch actuators. In order to impart zero net loads on the vehicle's interface to the test stand, the pitch and yaw commands on engines for steps and frequency responses were commanded in the predicted geometric null space such that opposing engines would vector simultanously towards or away from each other. An additional max-rate circular gimbal test was performed during the low-throttle portions of the burn. This circular gimbal test served to demonstrate the full rate capability of the TVC system for low throttle conditions with the newly designed propellant-driven CAPU hydraulic supply.

Figure 19 shows the overall command and piston response data during the frequency and step portion of the profile. The frequency response was issued first with simultaneous gimbaling occuring in pitch and yaw axes. First the yaw axes executed discrete frequency sinusoids (at 0.4 degree amplitude) while pitch executed a series of 0.8 degree amplitude high frequency sines. Thereafter, the pitch axes performed the same low-frequency set while yaw executed the high frequency sines. The step responses followed the frequency response portion and were issued in descending amplitude in the yaw axes, then the pitch axes. All gimbaling was commanded so as to result in net zero lateral loading and minimize net loads on the vehicle and test stand.

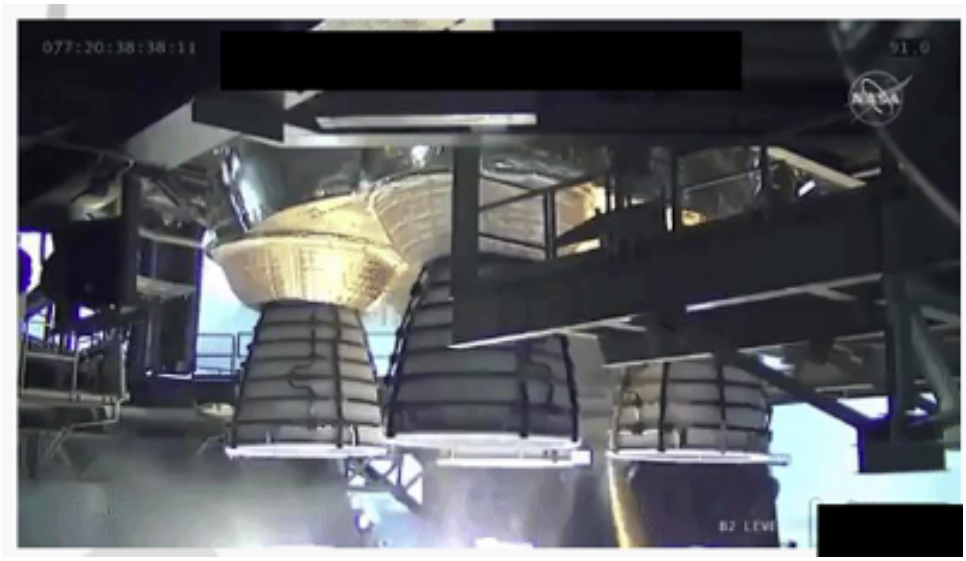

Figure 18. GRHF Engines Firing and Vectoring

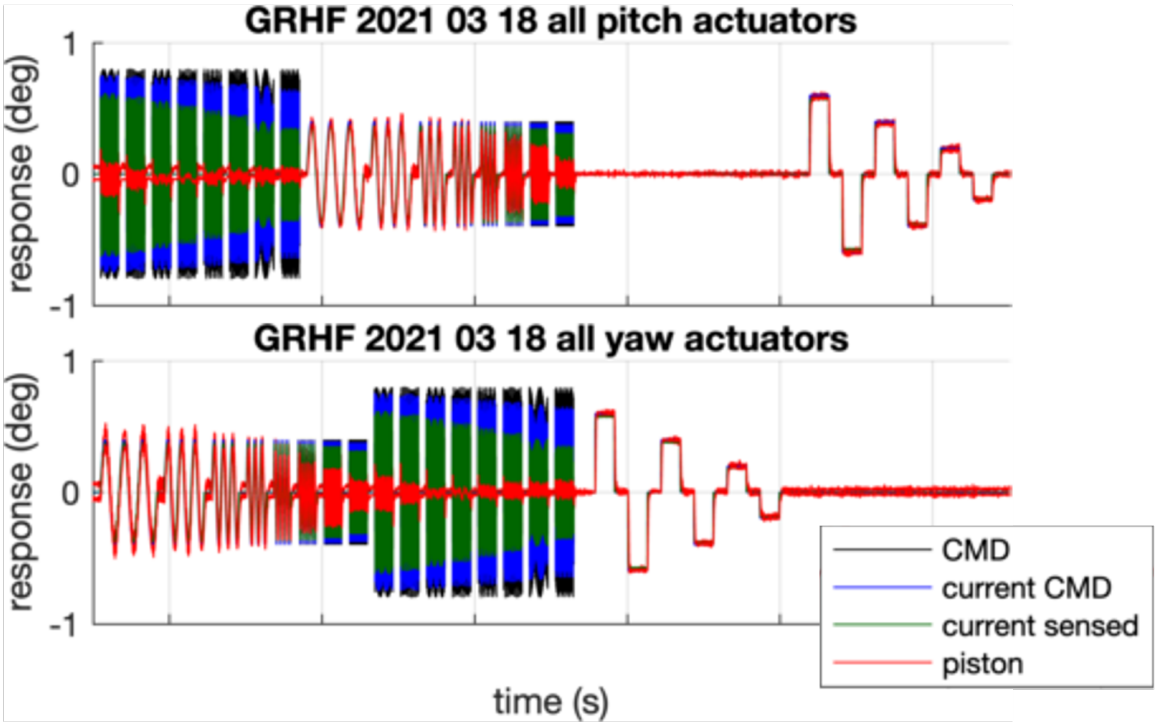

Figure 19. GRHF Command Schedule

Low Frequency Profile 0.4 deg Z-T-P		High Frequency Profile 0.8 deg Z-T-P	
Channel 1 (Hz)	Channel 2 (Hz)	Channel 1 (Hz)	Channel 2 (Hz)
0.4032	7.0-14.0 Hz increasing	7.0000	0.40-6.25 Hz increasing
0.5682		7.7286	
0.8333		8.5331	
1.1364		9.4213	
1.7857		10.4020	
2.5000		11.4847	
4.1667		12.6801	
6.2500		14.0000	

Figure 20. GRHF Command Schedule Frequencies

The frequencies and amplitude schedules for each portion are shown in Figure 20. The frequencies were selected to evenly distribute the frequencies across the target spectrum in logarithmic fashion with fine adjustments to ensure the peaks of the commands were aligned with the 20 ms command sample boundaries.

4.2 Frequency Response

The command-to-piston frequency responses for pitch and yaw are shown in Figure 21. The immediately noticeable difference was shift in the apparent piston notch (load resonance) frequency from the ambient test response, a significant and unexpected result. Using the approach employed following the ambient testing, the load stiffness parameter was adjusted from 110 klbf/in to 237 klbf/in in the linear Simplex TVC model, resulting in a 9.5 Hz notch in the piston response. Figure 21 shows a comparison of the pitch (left) and yaw (right) command to piston frequency responses for each engine in comparison to the load-stiffness-adjusted model. This notch shift between ambient and hot fire was subject of much study after the test was performed. Ultimately, detailed analysis determined this to be the result of the thrust loaded gimbal bearing and as well as other amplitude-dependent nonlinear characteristics[4] . While Shuttle MPTA testing was conducted in ambient and hot fire conditions, its highest frequency was lower than in the SLS test, and the quantization and sample rates were less favorable for reconstruction of the frequency response, so this particular load resonance shift was likely present, but not observed during the Shuttle program. As such, the SLS Green Run response was the first data that showed the drastic influence of thrust loading on the apparent load stiffness.

The second observation in the piston data is that the gain is decreased in the middle of the frequency ranges and the phase also deviates from the linear model predictions. This behavior can be attributed to the effects of friction[3] in the thrust-loaded gimbal bearing.

The frequency response for the averaged pitch (left) and yaw (right) engine responses derived from the string pot is shown in Figure 22. The engine responses show gain and phase deviations from the model in the mid band (as with the piston data), which is also attributed to thrust-loaded

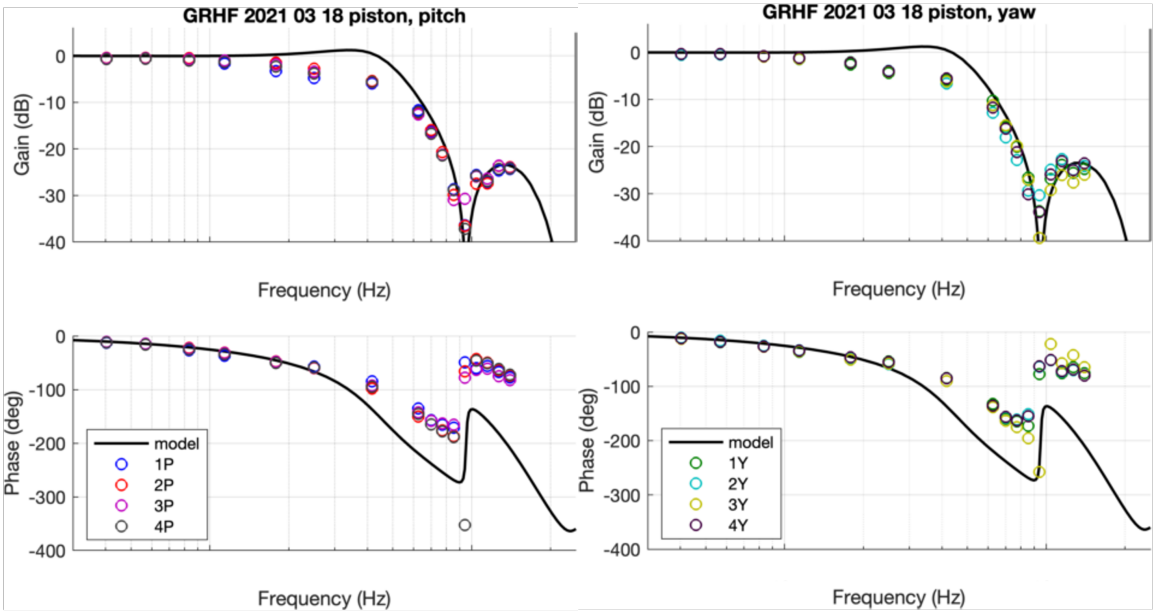

Figure 21. GRHF Piston Response

gimbal bearing friction. While the engine frequency responses at low frequency and in the higher frequency rolloff portion appear to match the linear model fairly well, it is important to note that the string-pot derived engine data could not be used to determine absolute gain and thus no conclusions about the influence of friction could be made. Section 5.1 contains further discussion of the string pot limitations and methods to approximate engine angles.

4.3 Step Response

The step responses for the each axis (top plots) and amplitude (each column) piston responses are shown alongside the load-stiffness adjusted linear models in Figure 23. A significantly more damped response is immediately apparent as a result of thrust-loaded gimbal friction.

The step response for the string pot derived engine angle responses are derived from the processing technique discussed in Section 4.1 and shown in Figure 24. In comparison to the linear models tuned for the notch stiffness seen in the frequency response, the step responses exhibit a significantly damped response due to gimbal friction.

4.4 Discussion of Results

Subsequent test-correlated modeling and analysis determined that the damped step response characteristics are suitably predicted by advanced models of gimbal friction (extensions of the Dahl[8] and LuGre[9] approaches) coupled with a higher fidelity representation of the gimbal bearing structure. These model enhancements readily show the gain and phase effects observed in the mid-band of the test frequencies during test.[3]

While Shuttle MPTA testing did not have a measurement of the engine position, the friction-augmented models show piston responses that compare favorably to the trends observed in Shuttle data in both step and frequency response.[1] Shuttle testing also included differential pressure measurement that could determine actuator load, and conducted ramp command testing to elucidate

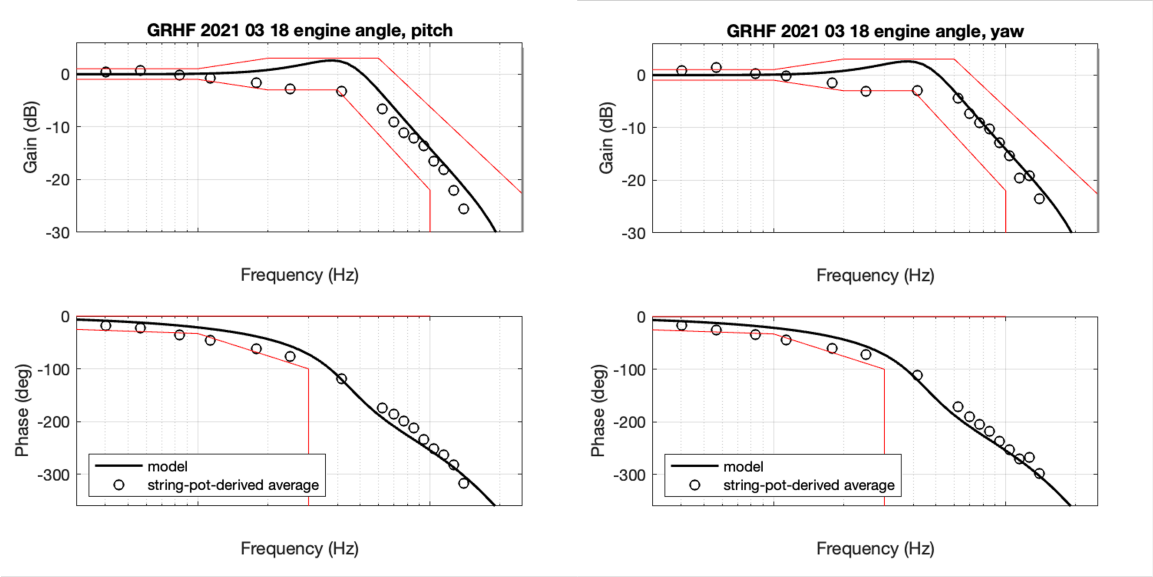

Figure 22. GRHF String-Pot Derived Engine Response

friction parameters. The test-derived friction coefficients were siginificant, but debate continued throughout the Shuttle program as to how to incorporate these data into flight control models.

Initially, the SLS flight control team developed design products under the long standing MSFC flight control and TVC community assumption that friction could be neglected in flight. Indeed, Shuttle documentation indicates that the MPTA observed friction effects were not a flight control concern.[1] Furthermore, Shuttle flight data never exhibited the characteristic limit cycle in flight that would have strongly indicated the presence of Coulomb friction . As a result, little detailed analysis was conducted on the subject of gimbal friction during the Shuttle program, although informal documentation suggests that some engineers recommended investigating advanced friction modeling approaches.

In the SLS test program, the engine position data in conjunction with the piston data provided a more conclusive indication of gimbal friction, necessitating the use of advanced friction models.[3] The inclusion of bounding and test-anchored friction in the TVC models supported flight rationale by demonstrating that an in-flight LCO would be inconsequential for flight control stability and performance.[5] However, due to the constrained geometry, the string-pot-to-angle reconstruction method required an assumption of achieved engine angle and thus could not provide a firm indication of friction-influenced amplitude nonlinearity. Since the effect of friction on the total actuator gain is only observable in the engine angle, it was not until the Programmed Test Input (PTI) frequency response data was processed following Artemis I flight that such engine gain effects could be seen. These data and the performance during the highly successful Artemis I flight test are discussed in the companion paper.[5]

5 SUPPORTING TECHNIQUES AND ANALYSIS

This section describes the use and analysis of the string pots for reconstructing engine data as well as detailing the numerical describing function method of extracting frequency domain response data from the discrete sines executed in all the test environments shown herein.

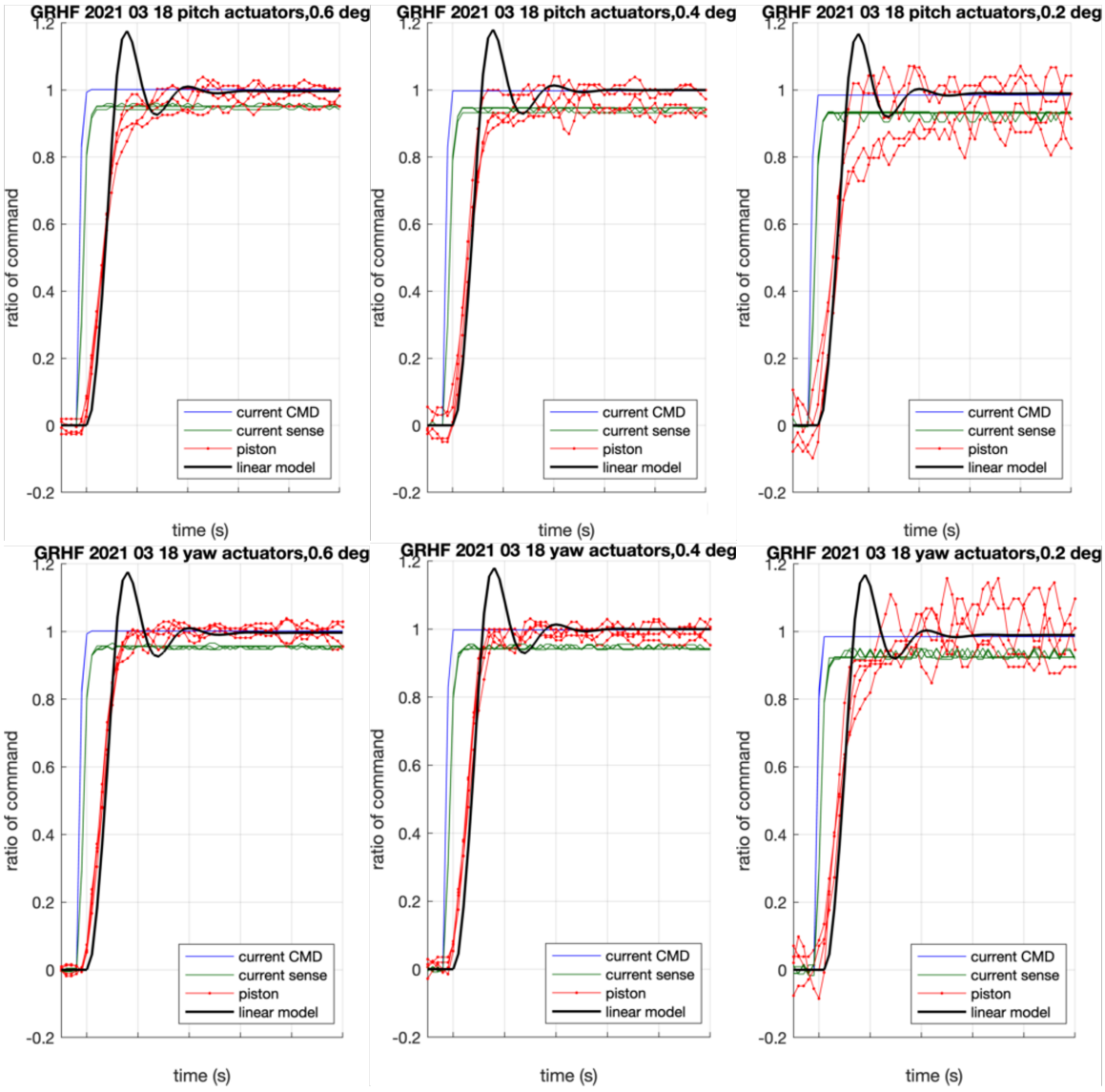

Figure 23. GRHF Piston Step Responses

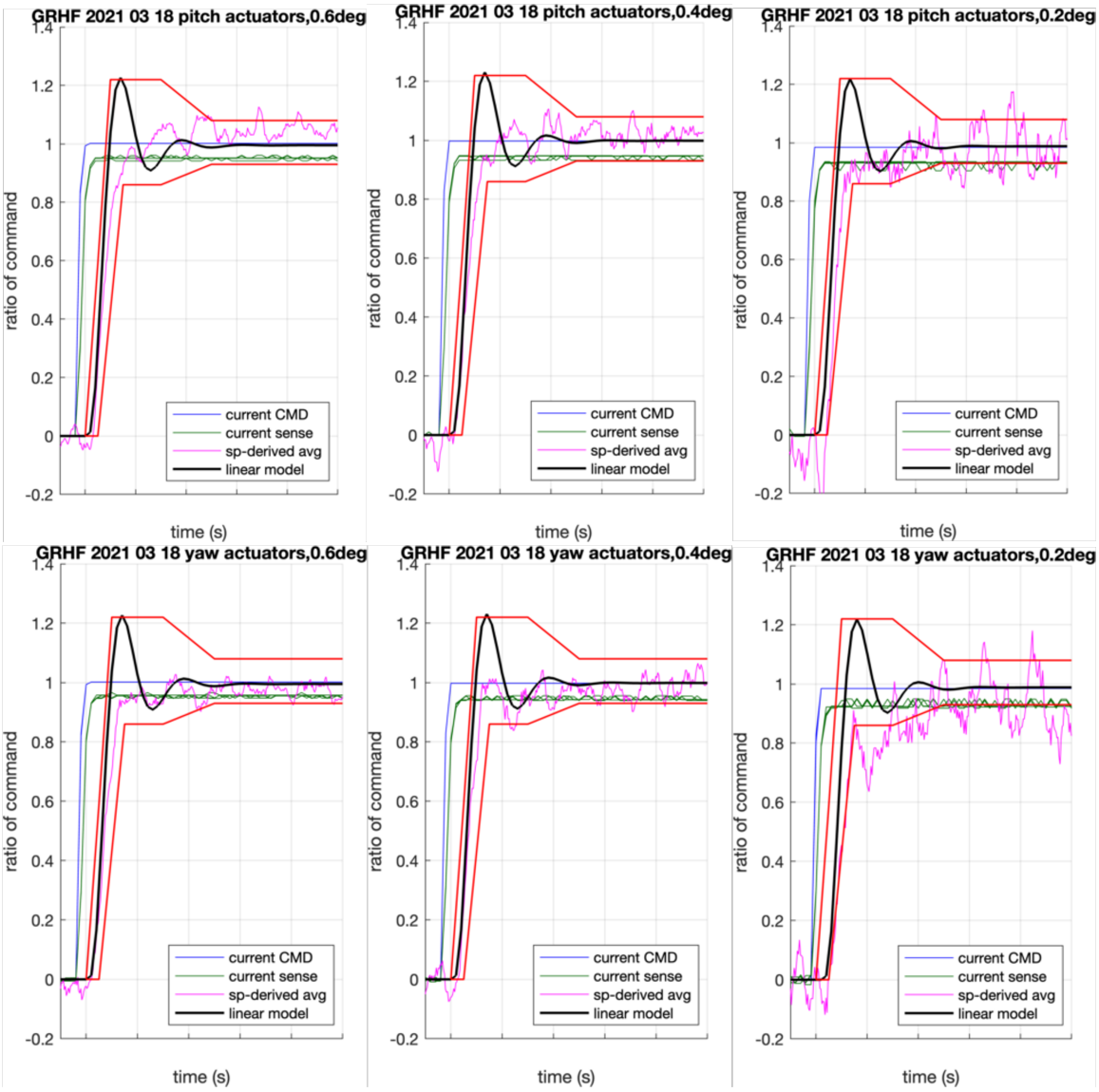

Figure 24. GRHF Engine Step Responses

5.1 String Potentiometers: Angle Conversions and Findings

The string potentiometer measurements were used on several TVC test stands in the MSFC 4205 2-axis test facility and provided a high precision and accurate means to determine the angular position of the engine load simulator along each actuator plane of motion. The sensor is comprised of a ruggedized housing from which a retractable steel cable can be extended by pulling on the eyelet attached to the cable end.

Prior to the ambient vectoring tests at the Stennis B-2 stand, string pots were installed with the sensor bodies attached to the engine section heatshield and the string end attached to bandclamps on available engine ducting . While not resulting in optimal geometry for determination of engine angles, the placement was the result of the limited line of sight availability in the engine section and acceptable means of attachment to the engine. Being installed above the heatshield, the string pots were protected from the thermal environments, did not require attachment to the nozzle, and were easily removed prior to shipment to KSC for flight. During hot fire, all 16 measurements devices survived the firing environment and produced uniquely valuable data despite limitations inherent in the measurement approach.

Several methods for determining the engine angles from the string pots were explored throughout the course of the Green Run test campaign.

During TC-7 ambient testing, even after precise measurements were taken of the end point locations relative to a known datum in the engine section, initial planar solutions were significantly scattered and did not match the expected commands or visual data. In Section 3 that shows the TC-7 final result, the authors settled on a best fit solution whereby the end points were solved to match expected motions during specific steady state motions. The end points were then used in planar transformations to convert from string length to angle. During hot fire testing, the end points both on the heat shield and engine section were expected to move as the entire structure deflects under thrust load, so the ambient derived end points would not be an accurate assumption for hot fire. To determine engine angles from string pot measurements during hot fire a variety of methods were employed to determine a best fit including using as-measured points and stress FEM predictions of the expected deflection of end points, 3-D solver using those end points, and finally a method that utilize a direct affine transform, described below. The affine transform resulted in the best solution and further led to the discovery that opposing engine pairs with like-mounted actuators resulted in a synchronized but symmetric/asymmetric roll motion that would cancel when data from those two engines were averaged. The final result of the affine and averaged transform produced the step frequency responses shown in Section 3. While the absolute value of the nozzle motion in response to commands could not be determined from the string pot data, the transient and frequency response characteristics provided invaluable data that helped uniquely identify characteristics associated with the unpexected responses. Neither ambient nor hot fire engine response data was available during the MPTA Shuttle program; only the piston data served as the closest available representation of the nozzle motion.

5.1.1 Affine Transformation of String Pots During Hot Fire The string length can be represented analytically as the norm of the difference between the non-rotating vector from the gimbal to the string pot spool, **u**, and the rotating vector from the gimbal to the string end on the engine, **v**. The pitch and yaw transform matrix is T. To further refine the sensor and end locations, a numerical optimizer searched for string end and spool positions that minimized the error between logged string length timeseries,l_n, and a simulated string length for the angles alpha and beta in command

time series, $g(t)$, using Equation (7). After identifying spool and end locations consistent with the data, engine angle estimates were obtained by finding the angles at each step of the time series that minimized the formula. Results could be further constrained by only searching in either pitch or yaw alone.

$$l_n = |\mathbf{u}_n - T(\alpha, \beta)\mathbf{v}_n| \tag{4}$$

$$[\alpha, \beta] = g(t) \tag{5}$$

$$\min \left(\sum_t \left(l_n(t) - |\mathbf{u}_n - T(g(t))\mathbf{v}_n| \right)^2 \right) \tag{6}$$

During hot fire testing, the end points both on the heat shield and engine section were expected to move as the entire structure deflected under thrust load. The endpoint error solving method used to process the ambient data proved less successful with the larger search volumes and higher noise environment on the thrust-shifted hot fire vehicle. Figure 25 shows that the changes in overall string length from ambient testing to hot fire are large relative to those due to the TVC test command profiles. The relationship between string lengths and associated engine angles are sufficiently linear over the +/-0.8 degree range of the hot fire TVC command sequence to consider fitting a linear transform to estimate engine angles. The affine transform preserves the rotation, scale, and shear capabilities of a two-dimensional geometric transform matrix, but is augmented to allow overall shift as well. The vector x can be transformed with the matrix A after augmentation with shifts in vector b to yield vector y. Static string pot data collected during hot fire seconds after step response settling were used with command angles to find a least-squares-fit affine transform to convert string pot lengths to estimated engine angles.

$$\begin{bmatrix} \mathbf{y} \\ 1 \end{bmatrix} = \left[\begin{array}{ccc|c} & A & & \mathbf{b} \\ 0 & \cdots & 0 & 1 \end{array} \right] \begin{bmatrix} \mathbf{x} \\ 1 \end{bmatrix} \tag{7}$$

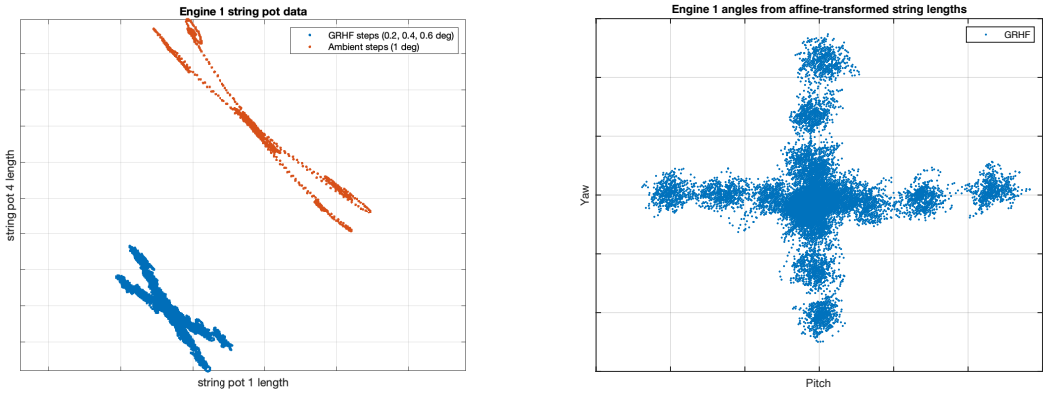

Figure 25. a. Scatter of string lengths from 2 string pots on engine 1 during ambient and hot fire testing. b. Scatter of engine angle estimates from string length data after application of best-fit affine transform.

Some engine roll motion is permitted by gimbal compliance during vectoring. While this is not expected to affect the thrust vector, the string pots geometries were sensitive to engine roll and there was a need to remove roll effects from the pitch and yaw engine angle estimates. The lack of static engine roll step data prevented the fitting of a three dimensional affine transform. Simulated string pot data applied to the fitted affine transforms demonstrated that roll projected to the yaw-pitch axes with one polarity for engines 1 and 3 and with opposing polarity for engines 2 and 4. Figure 26 shows the result of averaging the affine-transformed engine angle timeseries for complementary engines where the the roll artifacts are largely cancelled as a result of symmetric roll responses amongst the engines.

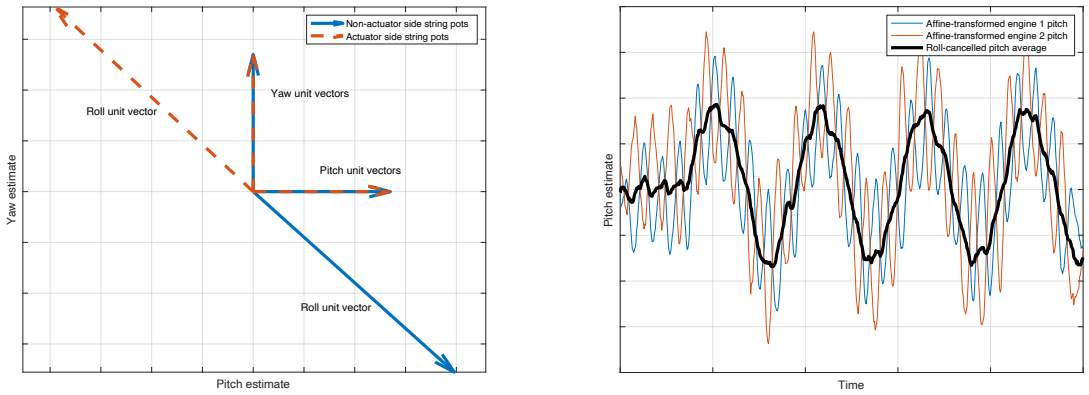

Figure 26. a. Roll, pitch, and yaw vectors projected into engine angle estimate plane for engines 1 & 4. b. Roll component nulling by combining pitch estimate timeseries from engines with complementary symmetry.

5.2 System Identification via Describing Functions (DF)

Describing function (DF) analysis is a useful tool for predicting sustained periodic solutions (limit cycles) of single-input, single-output nonlinear feedback dynamical systems, and the system identification technique used herein synthesizes a pointwise, numerically determined, complex-valued describing function

$$N\left(A,\omega\right) \tag{8}$$

as a function of input amplitude A and frequency ω, where the TVC actuator engine position and piston displacements are assumed to be described by a nonlinear system

$$\dot{\mathbf{z}} = f(\mathbf{z},u) \tag{9}$$

$$q = h(\mathbf{z},u) \tag{10}$$

with $\mathbf{z} \in \mathbb{R}^n$.

If given the input

$$u = A\sin\omega t \tag{11}$$

the output $q(t)$ is periodic as t increases, the nonlinearity in Equations (9-10) can be approximated by the first harmonic of a Fourier series expansion, i.e., a describing function. In the special case that f and h are linear functions of $\mathbf{z}$ and u, the describing function is equivalent to the usual complex-valued transfer function $H(j\omega) = q/u$.

It is often assumed in the use of describing functions that the nonlinearity must be single-valued and static, in which case $f = 0$ and $q = h(u)$; that is, the system has no dynamics. There is no restriction on the use of a dynamic nonlinearity in the feedback path so long as the describing function is computable (i.e., the nonlinear system is locally stable with respect to input perturbations), even if the describing function cannot be determined analytically.

In either a simulation or test environment, the exact sinusoidal describing function approximation $N(A_j, \omega_k)$ can be determined at the discrete amplitudes and frequencies A_j, ω_k using a trapezoidal integration approximation to compute the real Fourier coefficients[10] using a discrete-time (sampled) representation of $q(t)$ taken from the actuator output;

$$a_{jk} = \frac{2}{T_k} \int_{-T/2}^{T/2} q_{jk}(nt_s) \cos(\omega_k t)\, dt \tag{12}$$

$$b_{jk} = \frac{2}{T_k} \int_{-T/2}^{T/2} q_{jk}(nt_s) \sin(\omega_k t)\, dt \tag{13}$$

where t_s is the sample period (typically $20\,\mathrm{ms}$). The real and imaginary parts of N are then computed using

$$|N_{jk}| = \frac{\sqrt{a_{jk}^2 + b_{jk}^2}}{A_j} \tag{14}$$

and

$$\angle N_{jk} = \tan^{-1} \frac{a_{jk}}{b_{jk}}. \tag{15}$$

The phase is subsequently corrected for the sampling delay $t_s/2$. Since the computation of the Fourier coefficients is restricted to a single, known *a priori* signal, this method rejects frequencies outside the command frequency ω_k and recovers, in a least-squares sense, only the first harmonic of the output. In a test environment, this tends to reject the cross-talk effects from adjacent actuator degrees of freedom and provide resonably accurate phase response. In practice, it is necessary to pay careful attention to timing alignment to eliminate spurious phase effects, and the integration limits must be chosen to be a few time constants beyond the settling time of the system's transient response. The integration limits are extended over several periods, depending on available test time, in order to reduce the effects of zero-mean noise. Pre-test verification of the efficacy of the chosen input test signals is performed numerically using a linear model, for which N is equal to the transfer function.

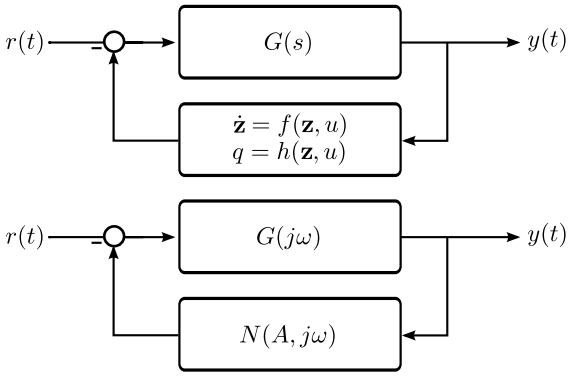

Figure 27. Original and describing function approximation of feedback nonlinearity

System identification in the form a describing function yields a useful tool for model validation, since the entire nonlinear system (the actuator DoF) can be replaced with a family of describing functions for stability analysis. The approximation N can be incorporated into the loop as in Figure 27. The Nyquist theorem predicts, but does not guarantee, the existence of a sustained periodic oscillation in the closed-loop system (a limit cycle) at a particular frequency ω and amplitude A if the linearized system return difference function satisfies the equality

$$1 + G(j\omega)N(A, j\omega) = 0, \tag{16}$$

for some $\omega = \omega_k$ and $A = A_j$. This leads to the well-known sinusoidal inverse describing function relationship

$$G(j\omega) = -\frac{1}{N(A, j\omega)}. \tag{17}$$

In practice, control stability analysis is performed by eliminating the additional frequency variable and evaluating the function $G(j\omega)N(A, j\omega)$ (Equation 16) over a set of discrete frequencies $\omega = \omega_k$, $k = 1, 2, \ldots, n$. Comparison of this function with the point $-1 + j0$ in the complex plane provides an equivalent criterion to Equation (17). At each unique amplitude A_j, the resultant curve can be interpreted similarly to a traditional Nichols plot, and provides a measure of describing function gain or phase margin with respect to the predicted LCO. This technique is referred to as "DF-in-the-loop".[11]

6 CONCLUSIONS

The SLS Core Stage TVC system utilized a number of Shuttle hertiage components, which were connected to a new command system and attached to a new structure. SLS's test of the integrated TVC system revealed response characteristics both known and unknown to the Shuttle engineers. The findings from test and subsequent analysis activities required a new way of thinking and the team worked with the new knowledge to build a strong rationale for first flight. The fidelity in the MSFC TVC test laboratory, late adds to testing during ambient conditions on the integrated vehicle, and Green Run Hot fire tests all provided critical elements. Using the outcomes from test, the SLS flight controls and TVC teams were able to firmly identify TVC system response characteristics, model their effects, and develop confident flight predictions for the flight of Artemis I.

ACKNOWLEDGMENTS

The authors recognize the support of Garry Lyles, John Blevins, Neil Otte, Mark West, Charlie Hall, Matt Strickland, Jason Bush, Joey Broome, Blake Stuart, Nick Johnston, Jesse McEnulty, Lila Paseur, David Young, Nathaniel Stepp, Lisa Bates, Boyd McNutt, Stan McDonald, Jeff Holmes, Bob Dougert, Adam Reinhart, Don Varanauski, Rick Zietler, and Shahram Namvari who throughought the SLS program worked to ensure the TVC test program was a success. This work was supported under contract number 80MSFC18C0011 for the NASA Marshall Space Flight Center.

REFERENCES

[1] McDermott et al. "Space Shuttle Ascent Flight Control Actuation Subsystem Data Book", SSD93D0595, Sept 30, 1993

[2] Gerstner, B. A. "MPT Engineering Analysis Second Interim Report Static Firings S/F-5A Through S/F-12" Rockwell Report STS 81-0254 May 1981

[3] Russell, C., Brouwer, J., Ryan, S., and Stepp, N. "Gimbal Bearing Friction in the Core Stage TVC System", AAS-23-154, American Astronautical Society GN&C Conference, Feb 2-8, 2023

[4] Moore, R. et al. "Structural Dynamics Observations in Space Launch System Green Run Hot Fire Testing", AAS-23-156, American Astronautical Society GN&C Conference, Feb 2-8, 2023

[5] Wall, J., Russell, C., Orr, J., Alaniz, A., Ryan, S., "Flight Performance and Stability of Space Launch System Core Stage Thrust Vector Control", American Astronautical Society GN&C Conference, Feb 2-8, 2023

[6] McMahan, T. and Harbaugh, J. "NASA Certifies SLS Rocket Laboratory To Test Flight Software for Artemis I" Online Article https://www.nasa.gov/exploration/systems/sls/news/sls-rocket-laboratory-certified-to-test-flight-software-for-artemis-I.html retrieved 2022 Dec 27

[7] Sontag, B. & Parks, Russel "Space Launch System (SLS) RS-25 Engine Pendulum Modal Test Report" NASA MSFC ET40 Report, SLS-DEV-20_024, Sept 28, 2020

[8] Dahl, P. R., "A Solid Friction Model," Space and Missile Systems Organization, TR-77-131, 1977.

[9] Olsson, H., Åström K.J., Canudas de Wit, C., Gäfvert, M., and Lischinksky, P., "Friction Models and Friction Compensation," *European Journal of Control*, vol. 4, no. 3, pp. 176-195, 1997.

[10] Klyde, D., McRuer, J., and Myers, T., "Pilot-Induced Oscillation Analysis and Prediction with Actuator Rate Limiting," J. Guidance, Control, and Dynamics, Vol. 20, No. 1, pp. 81–89, 1997.

[11] Orr, J. and Dennehy, C., "Analysis of the X-15 Flight 3-65-97 Divergent Limit Cycle Oscillation," AIAA J. Aircraft, Vol. 54, No. 1, pp. 135-148, 2016.

[12] Stuart, B., et al., "Overview of the SLS Core Stage Thrust Vector Control System Design," AAS 23-152, American Astronautical Society Guidance, Navigation, and Control Conference, February 2023.

[13] Orr, et al., "Advanced Modeling of Control-Structure Interaction in Thrust Vector Control Systems," AAS 23-153, American Astronautical Society Guidance, Navigation, and Control Conference, February 2023.

[14] Stuart, B., et al., "Core Stage TVC Systems Engineering Challenges in Reusing Heritage Hardware," AAS 23-154, American Astronautical Society Guidance, Navigation, and Control Conference, February 2023.